New Journal of Physics
The open-access journal for physics

Experimental implementation of partial symmetrization and anti-symmetrization of two-qubit states

Antonín Černoch[1], Jan Soubusta[1], Lucie Bartůšková[2], Miloslav Dušek[2] and Jaromír Fiurášek[2,3]

[1] Joint Laboratory of Optics of Palacký University and Institute of Physics of Academy of Sciences of the Czech Republic, 17 listopadu 50A, 779 07 Olomouc, Czech Republic
[2] Department of Optics, Faculty of Science, Palacký University, 17 listopadu 50, 772 00 Olomouc, Czech Republic
E-mail: fiurasek@optics.upol.cz

New Journal of Physics **11** (2009) 023005 (13pp)
Received 13 October 2008
Published 4 February 2009
Online at http://www.njp.org/
doi:10.1088/1367-2630/11/2/023005

Abstract. We report on experimental realization of tunable two-qubit state filtering using linear optical elements. The filter enables an arbitrary attenuation of either the symmetric or anti-symmetric part of the input two-qubit state. The device uses the encoding of qubits into polarization states of single photons and its operation is based on combination of single- and two-photon interference, selective attenuation and conditional detection. The filter is very flexible and the degree of symmetrization or anti-symmetrization can be easily set by means of variable attenuators. A full quantum process tomography of implemented operations was carried out and the results confirm very good performance of the filter.

[3] Author to whom any correspondence should be addressed.

Contents

1. Introduction

Quantum filters represent an essential tool for quantum information processing. These probabilistic non-unitary operations are required for diverse purposes ranging from discrimination, cloning and estimation of quantum states [1]–[3] to entanglement concentration and distillation [4, 5] and quantum error filtration [6]. An archetypal example of a quantum filter is the projector onto the anti-symmetric subspace of two qubits. Since this one-dimensional subspace is spanned by a maximally entangled singlet Bell state, such a filter can serve as partial Bell-state analyzer in quantum teleportation, entanglement swapping or other applications. In quantum optical implementations, where qubits are encoded into polarization states of single photons, the projection onto anti-symmetric subspace can be accomplished by two-photon interference on a balanced beam splitter [7]–[9]. A single photon appears in each output port of the beam splitter if and only if the photons are initially in the anti-symmetric singlet Bell state. The projection onto a singlet is thus unambiguously indicated by two-photon coincidence detection. On the other hand, if the input polarization state of the photons is symmetric, then they bunch and both emerge in the same output port of the beam splitter. This symmetrization via photon bunching has been exploited, e.g. for optimal universal quantum cloning [10].

Going beyond full symmetrization or anti-symmetrization, it is sometimes desirable to perform partial symmetrization or anti-symmetrization of the two-photon state. The latter can be accomplished by two-photon interference on an unbalanced beam splitter and coincidence observation of a single photon in each output port [11, 12]. The degree of anti-symmetrization can be adjusted by tuning the splitting ratio of the beam splitter. The partial symmetrization appears to be a more demanding operation in linear-optics framework as it requires a combination of single- and two-photon interference in a modified Mach–Zehnder (MZ) interferometer [13]. This kind of advanced quantum filter is demanded, e.g. in quantum information processing and quantum-state engineering. It can be used to accomplish various optimal cloning operations of polarization states of photons [11]–[14]. With a few additional photons and some linear optics the partial symmetrization of polarization states of two photons can emulate an amplification of photon pairs with an arbitrary gain [13]. Partial symmetrization can also serve for encoding of information into decoherence-free subspace of four-photon states [15].

In this paper, we report on the experimental realization of partial symmetrization and partial anti-symmetrization of polarization quantum states of two photons. The constructed linear-optical scheme is very versatile and the degree of symmetrization or anti-symmetrization can be easily tuned by adjusting the transmittances of variable attenuators. We characterize the filters

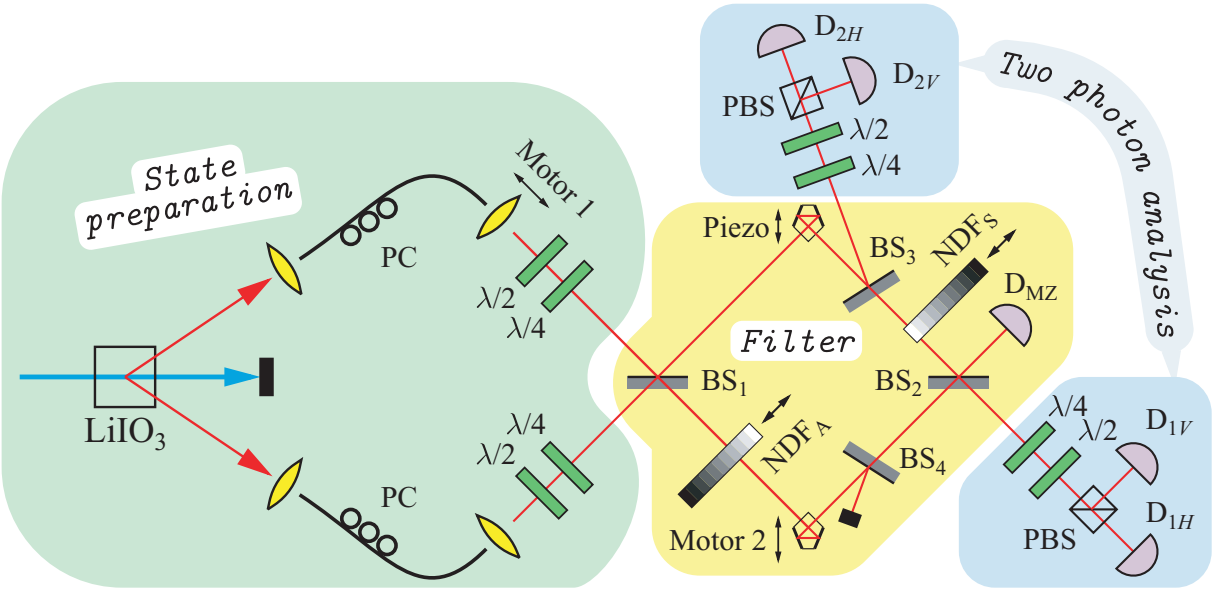

Figure 1. Experimental setup: PC, fiber polarization controller; BS, non-polarizing plate beam splitter; NDF, neutral density filter; PBS, polarizing cube beam splitter; $\lambda/2$ and $\lambda/4$, wave plates; D, describes a set composed of cut-off filter, collimating lens, single-mode fiber and avalanche photodiode.

by full quantum process tomography and verify high-fidelity operation over a broad range of degrees of symmetrization/anti-symmetrization. The rest of the present paper is organized as follows. In section 2, we explain the operating principle of the linear-optical partial symmetrizer and anti-symmetrizer. A detailed description of the experimental setup is provided in section 3. The experimental results are discussed in section 4. Finally, section 5 contains a brief summary and conclusions.

2. Theory

The setup, which is shown in figure 1, is essentially a MZ interferometer with additional balanced beam splitters and variable attenuators inserted into its arms. The interference of correlated and entangled photon pairs in an ordinary MZ interferometer has been studied in detail theoretically and experimentally in [16]–[19]. In the Heisenberg picture, the device can be described by linear input–output transformations for the annihilation operators [16]. Using this formalism one can show that the setup in figure 1 can conditionally implement the following (trace decreasing) operation on the polarization state of two photons [13, 20]:

$$\mathcal{V} = \sqrt{T_S}\,\Pi_+ + e^{i\phi}\sqrt{T_A}\,\Pi_-. \tag{1}$$

Here $\Pi_- = |\Psi^-\rangle\langle\Psi^-|$ and $\Pi_+ = I - \Pi_-$ are the projectors onto the anti-symmetric and symmetric subspaces of the two qubits, respectively, and I denotes the identity operator. The singlet state $|\Psi^-\rangle$ is one of the four Bell states, $|\Psi^\pm\rangle = \frac{1}{\sqrt{2}}(|H\rangle|V\rangle \pm |V\rangle|H\rangle)$, $|\Phi^\pm\rangle = \frac{1}{\sqrt{2}}(|H\rangle|H\rangle \pm |V\rangle|V\rangle)$, with $|H\rangle$ and $|V\rangle$ being horizontal and vertical linear polarization states of a single photon. ϕ denotes the phase difference between the two arms of the interferometer

formed by beam splitters BS_1 and BS_2. Quantities T_A and T_S are intensity transmittances of continuously variable neutral density filters NDF_A and NDF_S, respectively. Required intensity transmittances are set by sliding the NDFs into the optical beams. The scheme without NDFs was previously used by us to demonstrate a linear-optical two-qubit partial SWAP gate [20]. By adding the NDFs into the interferometer arms, we significantly increase the flexibility of the scheme and gain access to all operations of the form (1). In particular, by setting $T_S = 1$ and $\phi = 0$ we get the partial symmetrization operator

$$\mathcal{V}_S = \Pi_+ + \sqrt{T_A}\,\Pi_-. \tag{2}$$

Similarly, for $T_A = 1$ and $\phi = 0$ we get the partial anti-symmetrization operator

$$\mathcal{V}_A = \sqrt{T_S}\,\Pi_+ + \Pi_-. \tag{3}$$

The device operates in the coincidence basis [21] and the quantum filtering is successfully performed if a single photon is detected in each signal output port. The essence of the operation of the device is the two-photon interference on the first balanced beam-splitter BS_1, which separates symmetric and anti-symmetric two-photon states. Photons in anti-symmetric singlet Bell state $|\Psi^-\rangle$ anti-bunch on BS_1 so a single photon passes through each arm of the MZ interferometer. However, if the impinging photons are in a symmetric state then they bunch and both have to travel through the upper arm of the interferometer in order to reach the signal output ports. Thus by attenuating the beam in the lower arm, one can selectively suppress the contribution of the anti-symmetric component of the state. On the other hand, the attenuation of the beam in the path between BS_3 and BS_2 selectively suppresses only the symmetric states.

The scheme employed in our experiment is simple and flexible since T_A and T_S can be tuned merely by adjusting the variable attenuators. This comes at the expense of a somewhat reduced success probability of the scheme. We can define the intrinsic success probability of partial symmetrization, P_+, as the probability of success for input symmetric states. Similarly, we define the success probability of partial anti-symmetrization, P_-, as probability of success for input anti-symmetric singlet Bell state $|\Psi^-\rangle$. For the scheme shown in figure 1, the probabilities P_+ and P_- do not depend on degrees of symmetrization or anti-symmetrization T_A and T_S, respectively, and we have

$$P_+ = P_- = \frac{1}{8}. \tag{4}$$

The success probability can be enhanced by using a scheme with unbalanced beam splitters. Partial anti-symmetrization can be accomplished by two-photon interference on a single unbalanced beam splitter [11, 12] yielding intrinsic success probability $P_- = 1$ for all degrees of anti-symmetrization. For partial symmetrization, we cannot reach $P_+ = 1$ with linear optics only, but we can achieve

$$P_+ = \frac{1}{T_A^2}\left(1 - \sqrt{1 - T_A}\right)^2. \tag{5}$$

To reach this probability, we have to use a MZ interferometer composed of unbalanced beam splitters with splitting ratios depending on T_A [13]. Such an approach might thus be suitable if one needs a specific degree of symmetrization but is impractical if one wants an easily tunable device.

3. Experimental setup

Our experimental setup is shown in figure 1. It consists of three parts: the first one is the source of time-correlated photon pairs, the second one represents the filter itself and the last part is the detection block that serves for two-photon polarization analysis.

The main component of the first part is an $LiIO_3$ nonlinear crystal. It is pumped by a cw Kr-ion laser at the wavelength of 413 nm with power of 120 mW. Pairs of photons centered at 826 nm are generated in the process of type-I spontaneous parametric down conversion. The down-converted photons are coupled into two single-mode fibers which serve as spatial filters and then they are released back to free space. The polarization transformation introduced by the fibers is compensated by polarization controllers (PC) and the desired polarization state of each photon is set by means of half- and quarter-wave plates.

The device for two-qubit state filtering is formed by a bulk MZ interferometer with two additional beam splitters and two neutral density filters (NDFs) in each arm. The first signal output of the device is the lower port of beam-splitter BS_2, i.e. the output of MZ interferometer. The second signal output of the device is the beam reflected by beam-splitter BS_3 out of the upper arm of the MZ interferometer. BS_4 serves just to balance the losses in both interferometer arms. Adjustable additional losses in the interferometer are introduced by the NDFs. The NDF_S introduces losses in the upper arm behind BS_3 so it partially filters out a symmetric component of the input state, whereas attenuator NDF_A, which is placed in the lower arm, reduces the anti-symmetric component of the input state. The signal from the detector D_{MZ} is used for active stabilization of MZ interferometer phase ϕ. This output is polarization independent and monitors interference fringes.

The required operation is successfully implemented only when one photon goes by the first signal output (through the lower port of BS_2) and the other one goes by the second signal output (i.e. is reflected on BS_3). Thus, the analysis of the output two-photon state is performed by coincidence detection between two measurement blocks monitoring these outputs. Each detection block serves for a polarization measurement on a single photon and it consists of quarter- and half-wave plates and a polarizing beam splitter (PBS) which splits the photon state into horizontal and vertical polarization components. Before detection the beams are filtered spectrally by cut-off filters at 780 nm, and geometrically by single-mode fibers to ensure perfect overlap of the spatial modes in a free-space part of the setup. Signals from avalanche photodiodes are processed by four-input coincidence logic module to receive information about simultaneous detection of photon pairs.

The alignment of the setup is done in three steps. First, proper operation of the photon-pair source is verified. A separate fiber beam splitter is used to overlap the two photons of individual pairs and to measure two-photon interference in a Hong–Ou–Mandel (HOM)-type interferometer (not shown in figure 1) [22]. In this configuration, we have typically 11 000 coincidence counts per second out of the dip whose visibility is about 97%. Then the fiber beam splitter is replaced by two 5 m long fibers. Two PCs on the fibers serve to adjust horizontal linear polarizations at the output of the fibers. In the second step, the beam is blocked between beam splitters BS_3 and BS_2 and the overlap of the beams on the first beam-splitter BS_1 is optimized. We scan the HOM interference dip measuring coincidences between detectors D_{1H} and D_{2H} as a function of Motor 1 position. In this configuration, we observe about 150 coincidence counts per second in maximum and the visibility of HOM dip measured by time-to-amplitude converter (TAC) and single-channel analyzer (SCA) with 2 ns coincidence window is about 97%. The

substantial decrease of coincidence counts is due to the losses on the beam splitters BS_2, BS_3 and BS_4, and due to the non-perfect coupling to the single-mode fibers. Position of Motor 1 is set to the minimum of the dip. As a last preliminary step we adjust the single-photon interference in the MZ interferometer. For this purpose, one input arm in the source is blocked by the shutter and the output beam-splitter BS_2 is precisely aligned. The lengths of the interferometer arms are roughly balanced by motorized translation of one pentagon prism (Motor 2) to obtain the highest visibility of the interference fringes. Required precise fringe phase is tuned by piezo-driven translation of the pentagon prism in the other arm. We typically observe second-order visibility about 98%.

This type of interferometer is rather stable, the overall phase drift is about π per hour. Nevertheless, due to the air flux and changing temperature gradients the phase slightly oscillates. Therefore the interferometer must be actively stabilized in 20 s intervals [20]. The active stabilization procedure is performed as follows: the shutter blocks one arm in the source and with the help of signal from detector D_{MZ} the zero phase position is updated.

4. Results

Our experiment involved two sets of measurements: the first one for partial symmetrization with $T_S = 1$ and $T_A = 0$, 0.2, 0.4, 0.6, 0.8; and the second for partial anti-symmetrization with $T_A = 1$ and decreasing T_S from 1 to 0 with the decrement of 0.2. In both cases the phase ϕ was kept zero. For both sets, we simultaneously measured four two-photon coincidence counts between detectors $D_{1H}\&D_{2H}$, $D_{1V}\&D_{2V}$, $D_{1H}\&D_{2V}$ and $D_{1V}\&D_{2H}$, always for 3×3 combinations of polarization measurement bases in the two output arms. Namely, we measured projections onto horizontal/vertical (H/V), diagonal/anti-diagonal (D/A) and right/left circular (R/L) polarizations. The diagonal and anti-diagonal linear polarization states are defined as $|D\rangle = \frac{1}{\sqrt{2}}(|H\rangle + |V\rangle)$ and $|A\rangle = \frac{1}{\sqrt{2}}(|H\rangle - |V\rangle)$ and the right- and left-handed circular polarizations read $|R\rangle = \frac{1}{\sqrt{2}}(|H\rangle + \mathrm{i}|V\rangle)$ and $|L\rangle = \frac{1}{\sqrt{2}}(|H\rangle - \mathrm{i}|V\rangle)$. The unequal detector efficiencies were compensated by proper re-scaling of the measured coincidence counts [23]. Each measurement was done for 36 different input product states. Namely, for 6×6 combinations of polarization states $|H\rangle$, $|V\rangle$, $|D\rangle$, $|A\rangle$, $|R\rangle$ and $|L\rangle$ of each input photon. This complex measurement provided us with tomographically complete data enabling full characterization of the implemented operation by quantum process tomography [24]–[28] as well as reconstruction of the density matrices of output states for each used input state. For each setting we accumulated data for 15 s. After each accumulation a new polarization projection was set and the active stabilization of the MZ interferometer was always performed.

Any quantum operation $\mathcal{E}$ can be fully described by a completely positive (CP) map. According to the Jamiolkowski–Choi isomorphism, any CP map can be represented by a positive semidefinite operator χ on the tensor product of input and output Hilbert spaces $\mathcal{H}_{in}$ and $\mathcal{H}_{out}$. The operator χ is defined by the action of $\mathcal{E}$ on one part of a maximally entangled state. In our case this entangled state can be written as a tensor product of two Bell states $|\Phi^+\rangle_{AA'} \otimes |\Phi^+\rangle_{BB'}$, where A, B and A', B' label the input and output qubits, respectively. We have

$$\chi = 4\mathcal{I}_{AB} \otimes \mathcal{E}_{A'B'}(|\Phi^+\rangle\langle\Phi^+|_{AA'} \otimes |\Phi^+\rangle\langle\Phi^+|_{BB'}),$$

where $\mathcal{I}$ denotes the identity operation and the factor $4 = \dim \mathcal{H}_{in}$ ensures correct normalization. Note that χ is thus a square matrix with 16 rows and columns. The two-qubit input state ρ_{in}

Table 1. Performance of partial symmetrization operation. The table shows average and minimum fidelities of the output states, average and minimum purities of the output states, and quantum process fidelity for five different degrees of symmetrization.

T_A	F_{av}	F_{min}	$\mathcal{P}_{av}$	$\mathcal{P}_{min}$	F_χ
0	0.939	0.860	0.911	0.767	0.935
0.2	0.942	0.884	0.939	0.834	0.923
0.4	0.945	0.887	0.934	0.825	0.932
0.6	0.957	0.925	0.951	0.880	0.943
0.8	0.958	0.919	0.954	0.868	0.945

Table 2. Performance of partial anti-symmetrization operation. The table shows average and minimum fidelities of the output states, average and minimum purities of the output states, and quantum process fidelity for six different degrees of anti-symmetrization.

T_S	F_{av}	F_{min}	$\mathcal{P}_{av}$	$\mathcal{P}_{min}$	F_χ
1	0.962	0.915	0.941	0.856	0.949
0.8	0.952	0.908	0.932	0.860	0.937
0.6	0.952	0.905	0.924	0.854	0.937
0.4	0.942	0.909	0.908	0.838	0.925
0.2	0.924	0.886	0.877	0.804	0.901
0	0.862	0.799	0.771	0.673	0.819

transforms according to $\rho_{out} = \mathrm{Tr}_{in}[\chi(\rho_{in}^T \otimes I_{out})]$. Since we want to describe filter operations we have to consider general trace-decreasing CP maps and $\chi \geqslant 0$ is the only constraint imposed on χ. Combinations of different input states with measurements on the output quantum system represent effective measurements performed on $\mathcal{H}_{in} \otimes \mathcal{H}_{out}$. From the measured data, we can reconstruct χ for any setting of T_S and T_A using maximum likelihood (ML) estimation technique [28, 29]. To quantify the quality of the operation, we calculate process fidelity defined as $F_\chi = \mathrm{Tr}[\chi\chi_{id}]/(\mathrm{Tr}[\chi]\mathrm{Tr}[\chi_{id}])$. Here χ_{id} represents the ideal transformation (2) or (3). In particular, $\chi_{id} = \sum_{i,j,k,l=V,H} |i,j\rangle\langle k,l| \otimes \mathcal{V}|i,j\rangle\langle k,l|\mathcal{V}^\dagger$.

We have reconstructed partial symmetrization operation for five different values of T_A. As an illustration, in figure 2 we show real parts of χ for $T_A = 0.4,\ 0.2$ and 0. For comparison, also real parts of corresponding ideal χ_{id} are displayed. (Imaginary parts are close to zero with small noise.) Apparently, there is very good agreement between theory and experimentally obtained data. Process fidelities for all five values of T_A are given in the last column of table 1. They reach values well above 92%.

Similarly, we have reconstructed partial anti-symmetrization operation for six different values of T_S. Figure 3 shows real parts of χ of three reconstructed CP maps and three corresponding ideal CP maps for $T_S = 0.4,\ 0.2$ and 0. Process fidelities for all six values of T_S are displayed in table 2.

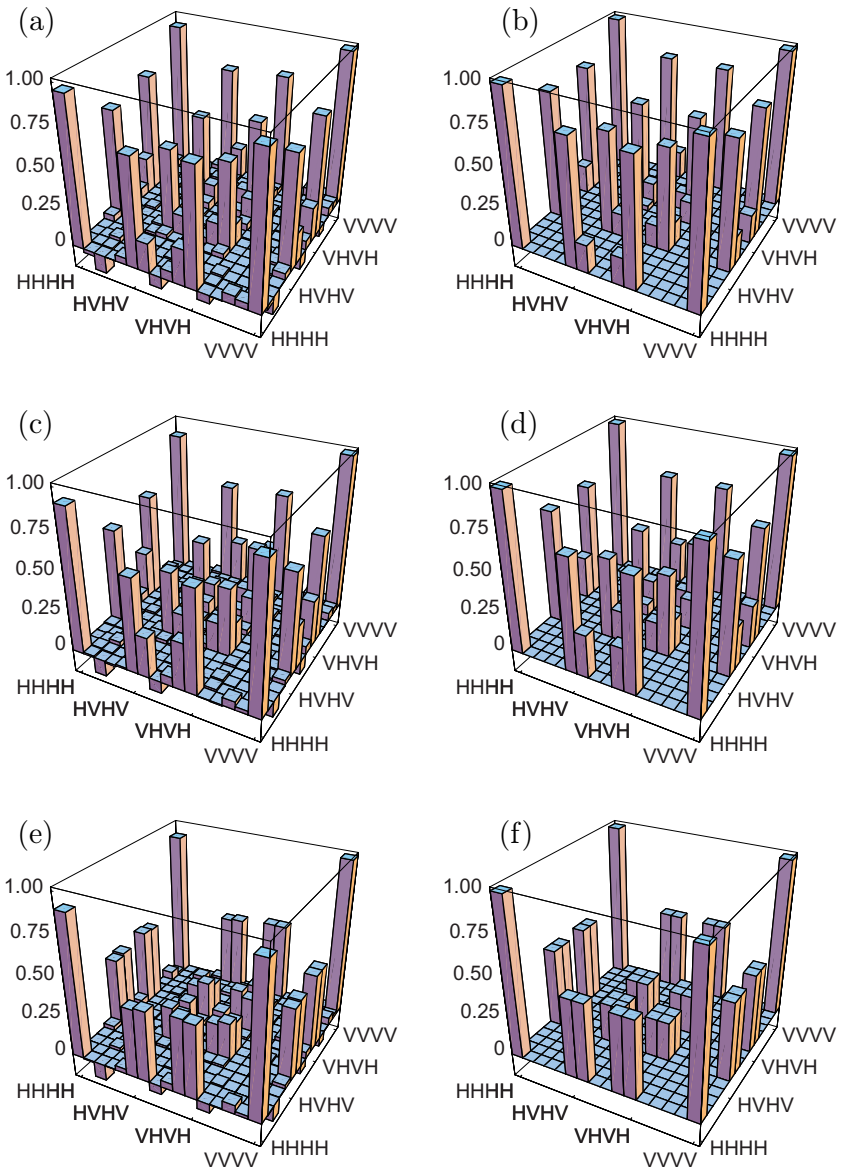

Figure 2. CP maps χ characterizing partial symmetrization operation. Real parts of the reconstructed CP map (left column) and ideal theoretical CP map (right column) are shown for $T_{\mathrm{A}} = 0.4$ (a, b), $T_{\mathrm{A}} = 0.2$ (c, d) and $T_{\mathrm{A}} = 0$ (e, f). In all cases $T_{\mathrm{S}} = 1$.

Figures 2 and 3 contain complete information on the implemented operation, but this information is scattered among many nonzero matrix elements. In order to capture the essential features of the studied operations we can restrict ourselves to a two-dimensional subspace $\mathcal{H}_2$ spanned by the states isomorphic to full symmetrization and full antisymmetrization, respectively,

$$|\pi_+\rangle = \frac{1}{\sqrt{3}}(|\Phi^+\rangle|\Phi^+\rangle + |\Phi^-\rangle|\Phi^-\rangle + |\Psi^+\rangle|\Psi^+\rangle),$$
$$|\pi_-\rangle = |\Psi^-\rangle|\Psi^-\rangle. \tag{6}$$

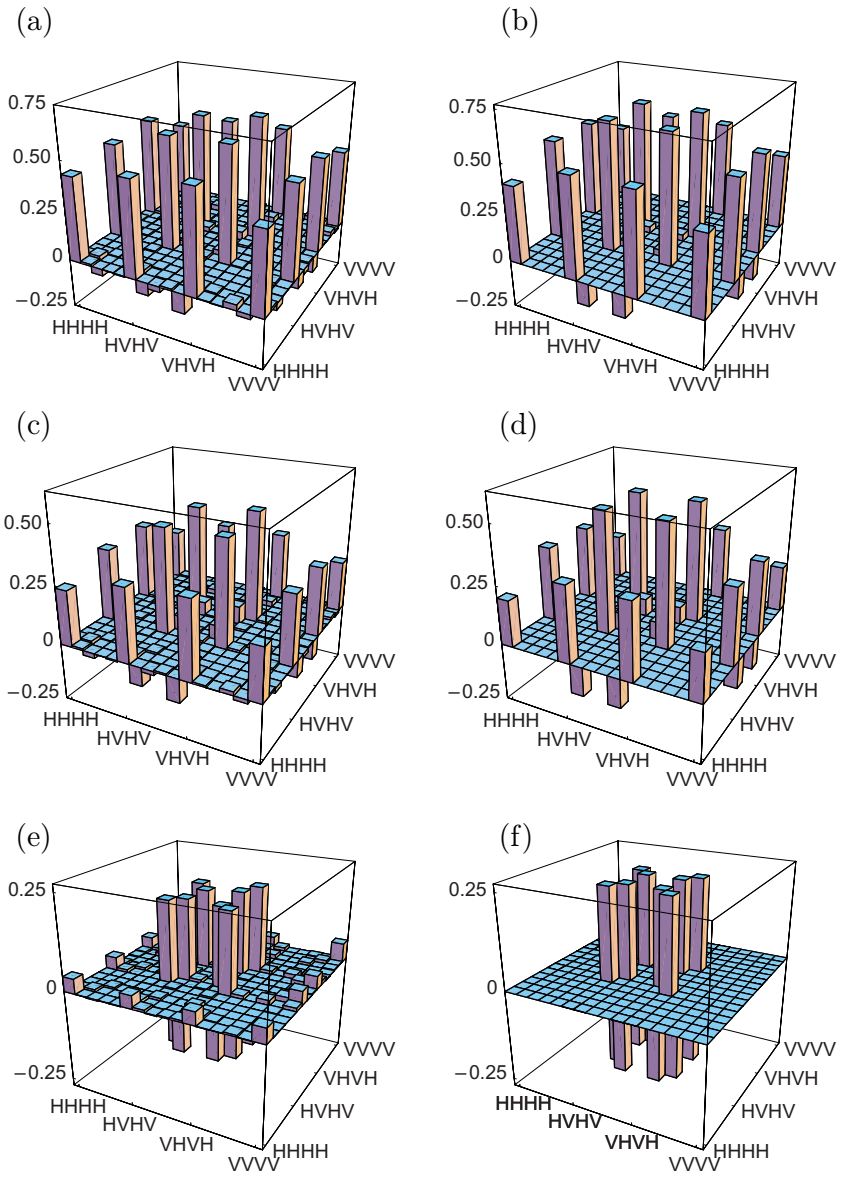

Figure 3. CP maps characterizing partial anti-symmetrization operation. Real parts of the reconstructed CP map (left column) and ideal theoretical CP map (right column) are shown for $T_S = 0.4$ (a, b), $T_S = 0.2$ (c, d) and $T_S = 0$ (e, f). In all cases $T_A = 1$.

The support of the ideal map χ_{id} is always restricted to this subspace so that for all degrees of symmetrization or anti-symmetrization it holds that

$$\mathrm{Tr}[\chi_{id}] = \mathrm{Tr}[\Pi_2 \chi_{id}], \tag{7}$$

where $\Pi_2 = |\pi_+\rangle\langle\pi_+| + |\pi_-\rangle\langle\pi_-|$ is the projector onto $\mathcal{H}_2$. For the reconstructed CP maps χ, we find that the fraction $f = \mathrm{Tr}[\Pi_2\chi]/\mathrm{Tr}[\chi]$ in all cases exceeds 0.94. The 2×2 matrices $\chi_2 = \Pi_2 \chi \Pi_2$ are plotted in figure 4 together with the corresponding ideal maps. The process of symmetrization/anti-symmetrization is clearly visible in the figure. The magnitude of the

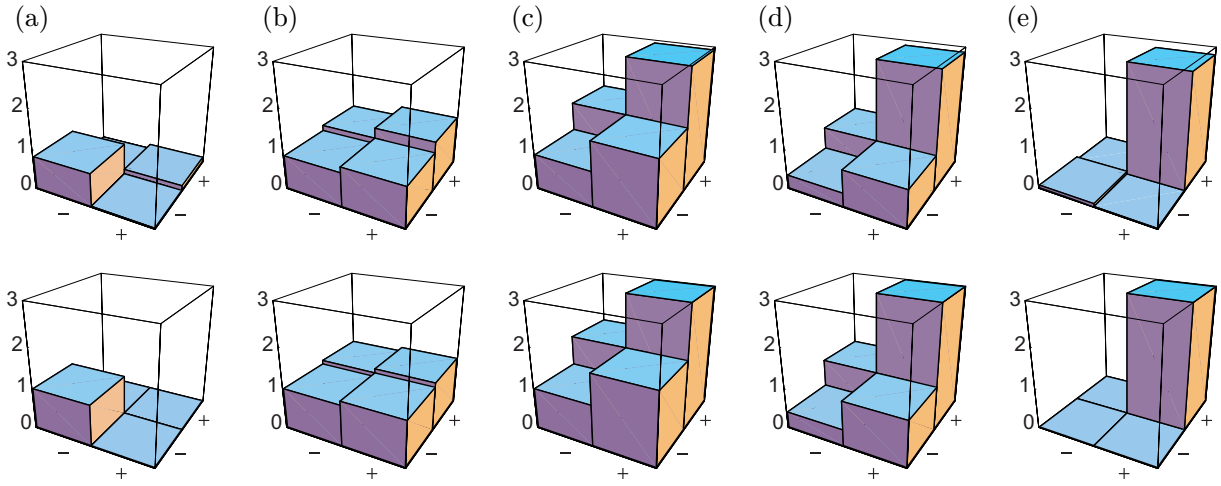

Figure 4. Two-dimensional projection χ_2 onto subspace spanned by $|\pi_+\rangle$ and $|\pi_-\rangle$. The upper row shows real parts of reconstructed CP maps and the lower row presents real parts of the ideal CP maps for comparison. The imaginary parts were negligible for the reconstructed maps and they vanish for the ideal maps. The results are shown for full anti-symmetrization $T_S = 0$, $T_A = 1$ (a), partial anti-symmetrization $T_S = 0.4$, $T_A = 1$ (b), identity operation $T_S = T_A = 1$ (c), partial symmetrization $T_S = 1$, $T_A = 0.4$ (d) and full symmetrization $T_S = 1$, $T_A = 0$ (e).

off-diagonal elements of reconstructed χ_2 is somewhat reduced with respect to the ideal map. This is a signature of a partial loss of coherence between the symmetric and anti-symmetric parts of the output states, which thus become mixed.

Further, we have reconstructed the density matrices of output two-photon states corresponding to all product input states composable from single photon polarization states $|H\rangle$, $|V\rangle$, $|D\rangle$, $|A\rangle$, $|R\rangle$ and $|L\rangle$. This was done for all values of T_S and T_A. As an example, in figure 5 we show complete reconstructed density matrices of output states corresponding to an input state $|R\rangle|L\rangle$. In this figure there are five different operations considered: full anti-symmetrization ($T_S = 0$, $T_A = 1$), partial anti-symmetrization ($T_S = 0.4$, $T_A = 1$), identity ($T_S = T_A = 1$), partial symmetrization ($T_S = 1$, $T_A = 0.4$) and full symmetrization ($T_S = 1$, $T_A = 0$). In panel (a) one can easily recognize a singlet Bell state $|\Psi^-\rangle$. On the other hand, in panel (e) there is a well recognizable triplet Bell state $|\Phi^+\rangle$. In panel (c), which corresponds to identity operation, the original input state is well reproduced. By feeding the input of the full symmetrizer with input product states $|H\rangle|V\rangle$ and $|D\rangle|A\rangle$, we can generate the other two symmetric Bell states $|\Psi^+\rangle$ and $|\Phi^-\rangle$, respectively. We have also confirmed that, if subjected to full anti-symmetrization, all these input states yield an anti-symmetric singlet Bell state at the output.

An important parameter characterizing the performance of the device is the fidelity of output states ρ_{out} defined as $F = \langle\psi_{out}|\rho_{out}|\psi_{out}\rangle$, where $|\psi_{out}\rangle = \mathcal{V}|\psi_{in}\rangle/||\mathcal{V}|\psi_{in}\rangle||$ and $|\psi_{in}\rangle$ is the (pure) input state. Table 1 contains the values of state fidelities for partial symmetrization, table 2 lists the values for partial anti-symmetrization. In both tables, state fidelities F_{av} averaged over 36 output states corresponding to input product states $|j\rangle|k\rangle$, $j, k \in \{H, V, D, A, R, L\}$ as well as the minimum fidelities F_{min} among these 36 states are shown. Another important

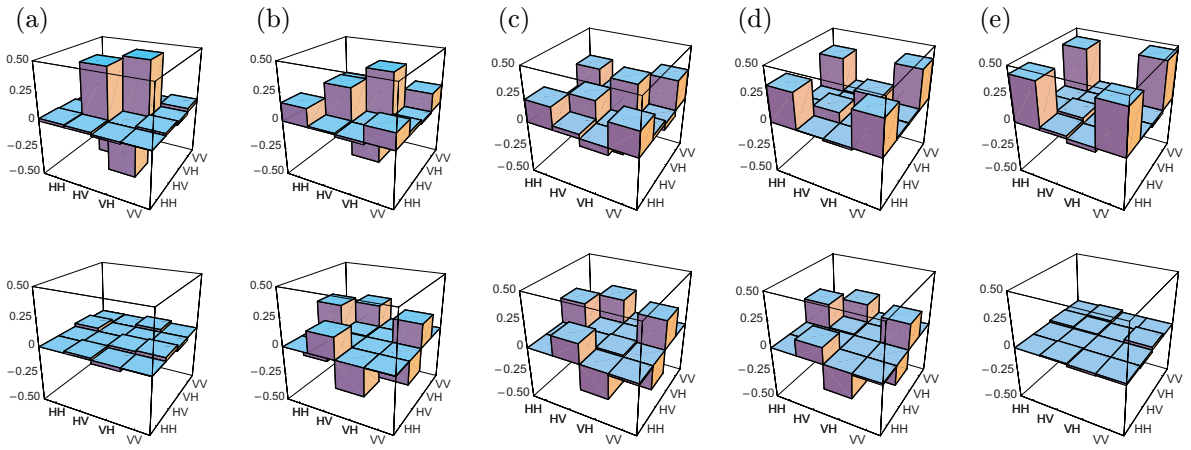

Figure 5. Reconstructed density matrix of the output state for input product state $|R\rangle|L\rangle$ and various levels of anti-symmetrization/symmetrization. The upper and lower rows display real and imaginary parts of the reconstructed density matrices, respectively. The results are shown for full anti-symmetrization $T_S = 0$, $T_A = 1$ (a), partial anti-symmetrization $T_S = 0.4$, $T_A = 1$ (b), identity operation $T_S = T_A = 1$ (c), partial symmetrization $T_S = 1$, $T_A = 0.4$ (d) and full symmetrization $T_S = 1$, $T_A = 0$ (e).

characteristic is the purity of the output state ρ_{out}. It is defined as $\mathcal{P} = \mathrm{Tr}[\rho_{out}^2]$. If the input state is pure then the output state is expected to be pure as well. The average and minimal purities of output states are also given in tables 1 and 2. All these data confirm a very good performance of the device. Averaged purities are very close to the ideal value $\mathcal{P} = 1$. The lowest fidelities ($F_{av} = 0.862$) and purities ($\mathcal{P}_{av} = 0.771$) were obtained for full anti-symmetrization.

We can identify several factors that reduce the quality of the implemented quantum filters. The first limiting factor is the non-unit visibility of HOM interference on balanced beam-splitter BS_1. The second contribution to the noise stems from the imperfect stabilization of the MZ interferometer, the phase ϕ is not entirely constant but randomly fluctuates about its mean value $\langle\phi\rangle = 0$. The third major source of noise is given by accidental coincidences and dark counts. In the limit of total symmetrization or anti-symmetrization, the fluctuations of the phase shift ϕ do not play any role because one arm of the interferometer is always blocked. A simple model assuming only imperfect two-photon interference on BS_1 with visibility V predicts the following process fidelities F_+ and F_- of the symmetrization and anti-symmetrization, respectively,

$$F_+ = \frac{3}{4}\frac{1+3V}{1+2V}, \qquad F_- = \frac{1+3V}{4}. \tag{8}$$

Note, that the anti-symmetrization is much more sensitive to the visibility of two-photon interference on BS_1 than symmetrization. However, it turns out that the observed process fidelity of full anti-symmetrization ($F_\chi = 0.819$) cannot be explained only by the imperfect overlap of photons on BS_1, because the visibility of HOM dip measured with TAC/SCA reaches 97%. In fact, we find that the main source of noise in the present experiment is the accidental coincidence counts arising due to the rather large coincidence window (20 ns) of the detection electronics used for simultaneous measurement of four coincidences. These accidental

coincidences effectively reduce the visibility of HOM dip and they add background noise to all measured data. We estimate that by using better electronics with narrower coincidence window, the process fidelity of the full anti-symmetrization could be increased above 90%.

5. Conclusions

We have demonstrated linear optical quantum filters that allow to perform arbitrary partial symmetrization or anti-symmetrization of polarization state of two photons. The device is very flexible and the desired degree of symmetrization or anti-symmetrization can be easily set by means of variable attenuators. High-fidelity operation of the filters was verified by quantum process tomography. These advanced tunable quantum filters represent an important addition to the toolbox of available techniques for linear optical quantum information processing. They may find applications, e.g., in preparation of multiphoton entangled states [15] or in realization of optimal cloning of quantum states of photons [13].

Acknowledgments

We thank Nicolas J Cerf for many stimulating discussions. This research was supported by the projects LC06007, 1M06002 and MSM6198959213 of the Ministry of Education of the Czech Republic.

References

[1] Duan L-M and Guo G-C 1998 *Phys. Rev. Lett.* **80** 4999
[2] Clarke R B M, Chefles A, Barnett S M and Riis E 2001 *Phys. Rev.* A **63** 040305
[3] Fiurášek J 2006 *New J. Phys.* **8** 192
[4] Bennett C H, Bernstein H J, Popescu S and Schumacher B 1996 *Phys. Rev.* A **53** 2046
[5] Kwiat P G, Barraza-Lopez S, Stefanov A and Gisin N 2001 *Nature* **409** 1014
[6] Gisin N, Linden N, Massar S and Popescu S 2005 *Phys. Rev.* A **72** 012338
[7] Bouwmeester D, Pan J-W, Mattle K, Eibl M, Weinfurter H and Zeilinger A 1997 *Nature* **390** 575
[8] Mitchell M W, Ellenor C W, Schneider S and Steinberg A M 2003 *Phys. Rev. Lett.* **91** 120402
[9] Pan J-W, Chen Z-B, Zukowski M, Weinfurter H and Zeilinger A 2008 arXiv:0805.2853
[10] Scarani V, Iblisdir S, Gisin N and Acín A 2005 *Rev. Mod. Phys.* **77** 1225
[11] Filip R 2004 *Phys. Rev.* A **69** 052301
[12] Filip R 2004 *Phys. Rev.* A **69** 032309
[13] Fiurášek J and Cerf N J 2008 *Phys. Rev.* A **77** 052308
[14] Zhao Z, Zhang A-N, Zhou X-Q, Chen Y-A, Lu C-Y, Karlsson A and Pan J-W 2005 *Phys. Rev. Lett.* **95** 030502
[15] Gong Y-X, Zou X-B, Niu X-L, Li J, Huang Y-F and Guo G-C 2008 *Phys. Rev.* A **77** 042317
[16] Campos R A, Saleh B E A and Teich M C 1990 *Phys. Rev.* A **42** 4127
[17] Rarity J G, Tapster P R, Jakeman E, Larchuk T, Campos R A, Teich M C and Saleh B E A 1990 *Phys. Rev. Lett.* **65** 1348
[18] Larchuk T S, Campos R A, Rarity J G, Tapster P R, Jakeman E, Saleh B E A and Teich M C 1993 *Phys. Rev. Lett.* **70** 1603
[19] Larchuk T S, Teich M C and Saleh B E A 1995 *Phys. Rev.* A **52** 4145
[20] Černoch A, Soubusta J, Bartůšková L, Dušek M and Fiurášek J 2008 *Phys. Rev. Lett.* **100** 180501
[21] Ralph T C, Langford N K, Bell T B and White A G 2002 *Phys. Rev.* A **65** 062324
[22] Hong C K, Ou Z Y and Mandel L 1987 *Phys. Rev. Lett.* **59** 2044

[23] Soubusta J, Bartůšková L, Černoch A, Fiurášek J and Dušek M 2007 *Phys. Rev.* A **76** 042318
[24] Poyatos J F, Cirac J I and Zoller P 1997 *Phys. Rev. Lett.* **78** 390
[25] Chuang I L and Nielsen M A 1997 *J. Mod. Opt.* **44** 2455
[26] Fiurášek J and Hradil Z 2001 *Phys. Rev.* A **63** 020101
[27] Sacchi M F 2001 *Phys. Rev.* A **63** 054104
[28] Ježek M, Fiurášek J and Hradil Z 2003 *Phys. Rev.* A **68** 012305
[29] Paris M G A and Řeháček J (ed) 2004 *Quantum State Estimation* (*Lecture Notes in Physics* vol 649) (Berlin: Springer)